Chemistry–A European Journal

Supporting Information

Fe^{III}_{48}-Containing 96-Tungsto-16-Phosphate: Synthesis, Structure, Magnetism and Electrochemistry

Joydeb Goura,[a] Bassem S. Bassil,[a, b] Jasleen K. Bindra,[c] Iwona A. Rutkowska,[d] Pawel J. Kulesza,[d] Naresh S. Dalal,[c] and Ulrich Kortz*[a]

Supporting Information

Experimental Section

Reagents and Instrumentation

The POM precursor salt $K_{12}[H_2P_2W_{12}O_{48}]\cdot 24H_2O$ was prepared according to the published procedure and characterized by FT-IR spectroscopy.[S1] All other reagents were used as purchased without further purification. IR spectra were recorded as KBr pellets on a *Nicolet Avatar 370* FT-IR spectrophotometer operating between 400 - 4000 cm^{-1}. Thermogravimetric analysis (TGA) was carried out on a TA Instruments *SDT Q600* thermobalance with flow of nitrogen; the temperature was ramped from room temperature to 800 °C at a rate of 5 °C/min. Elemental analysis for **K-Fe$_{48}$** was performed by Institut des Sciences Analytiques, CNRS, Villeurbanne, France.

X-ray Crystallography

A single crystal of **K-Fe$_{48}$** was mounted on a Hampton cryoloop in light oil for data collection at 100 K. A Bruker Kappa *D8 APEX II CCD* single-crystal diffractometer with kappa geometry and a graphite-monochromated MoK_α radiation (λ_α= 0.71073 Å) was used for indexing and data collection. Data integration was performed using *SAINT*,[S3] and routine Lorentz and polarization corrections were applied. Multiscan absorption corrections were performed using *SADABS*.[S4] Direct methods (*SHELXS97*) successfully located the tungsten atoms, and successive Fourier syntheses (*SHELXL2014*) revealed the remaining atoms.[S5] Refinements were full-matrix least-squares against $|F^2|$ using all data. In the final refinement, all non-disordered heavy atoms (P, K, Fe, W) were refined anisotropically; oxygen atoms and disordered counter-cations were refined isotropically. No hydrogen atoms were included in the models. The crystallographic parameters for **K-Fe$_{48}$** given in the Table S1. Further details on the crystal structure investigations may be obtained via CSD-1895635. Figures S1 and S2 were prepared using *Diamond*, Version 3.2 (copyright Crystal Impact GbR).

Table S1. Crystal data and structure refinement for **K-Fe$_{48}$**.

Empirical formula	$Fe_{48}H_{916}K_{36}O_{876}P_{16}W_{96}$
Formula weight, g/mol	37172.79
Temperature (K)	100 (2)
Crystal system	*Triclinic*
Space group	*P*$\bar{1}$
a (Å)	25.654(3)
b (Å)	38.137(4)
c (Å)	41.590(4)
α (°)	113.739(3)
β (°)	90.052(3)
γ (°)	105.991(3)
Volume (Å^3)	35516(6)
Density (Mgm^{-3})	3.476
Abs. coef. (mm^{-1})	16.818
F(000)	35648
θ range (°)	3.397 to 20.816
Limiting indices	-25≤h≤25 -38≤k≤38 -41≤l≤41
Reflections collected	74012
Unique reflections [R_{int}]	51075 [0.1720]
Completeness to θ	99.5 (25.242)
Data / restraints /parameters	74012/6/3908
GOOF on F^2	1.007
R_1[a] (I>2σ(I))	0.1169
wR_2[b] (all data)	0.2851

[a] $R_1=\Sigma\|F_0\|-\|F_c\|/\Sigma|F_0|$, [b] $wR_2=[\Sigma w(F_0^2-F_c^2)^2/\Sigma w(F_0^2)^2]^{1/2}$

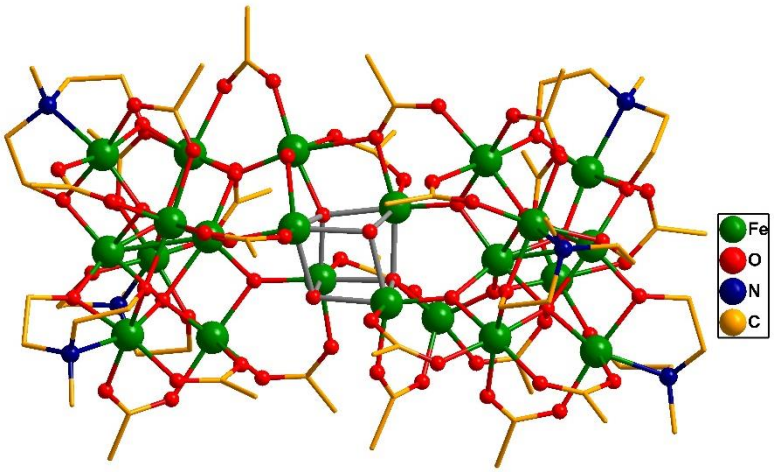

Figure S1. Ball-and-stick representation of $[Fe_{22}O_{14}(OH)_3(O_2CMe)_{21}(mda)_6]^{2-}$ (**Fe$_{22}$**).[S6]

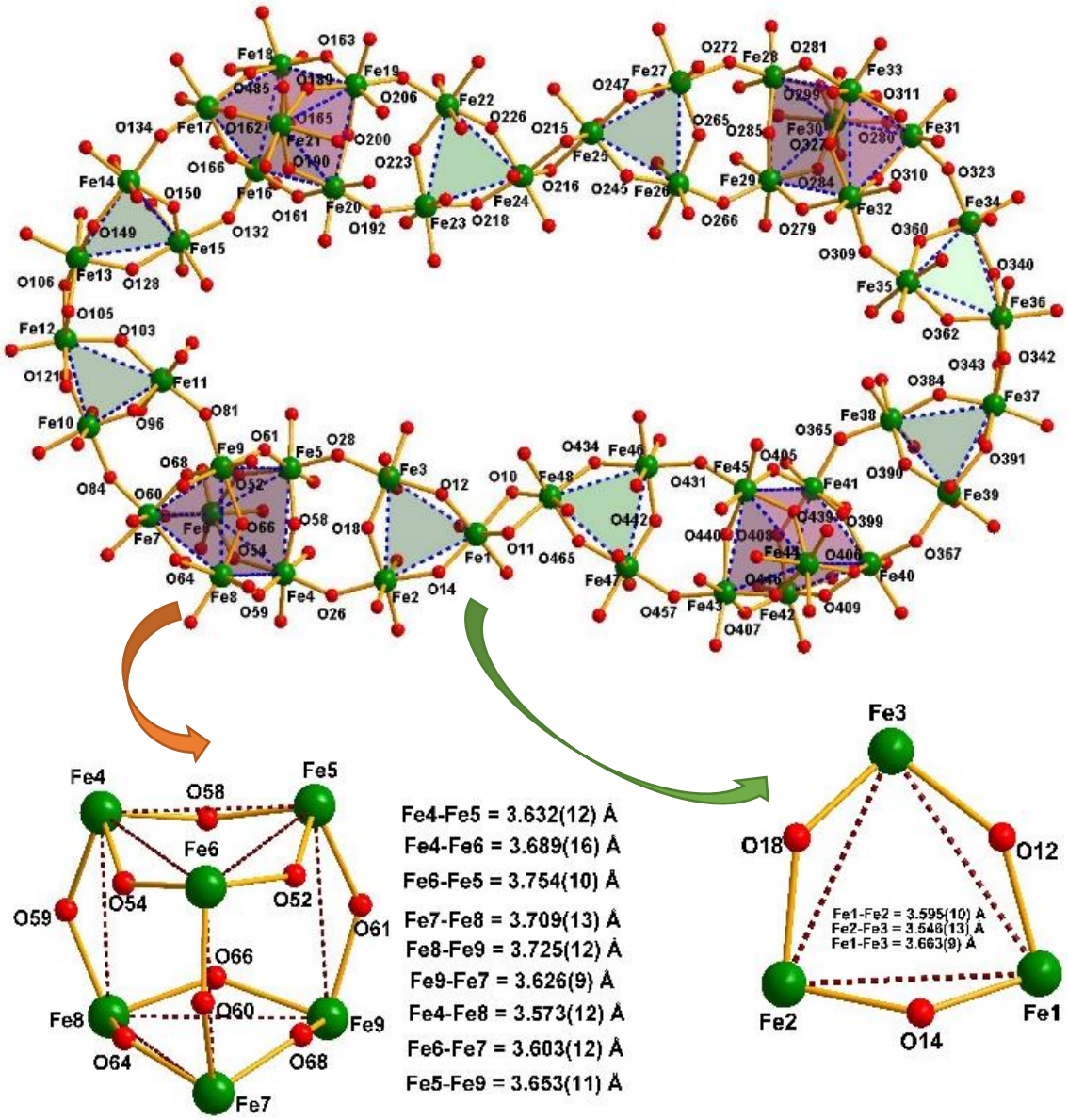

Figure S2. Core structure of **Fe_{48}** showing the triangular Fe_3 units and the trigonal-prismatic $Fe_6(OH)_9$ units.

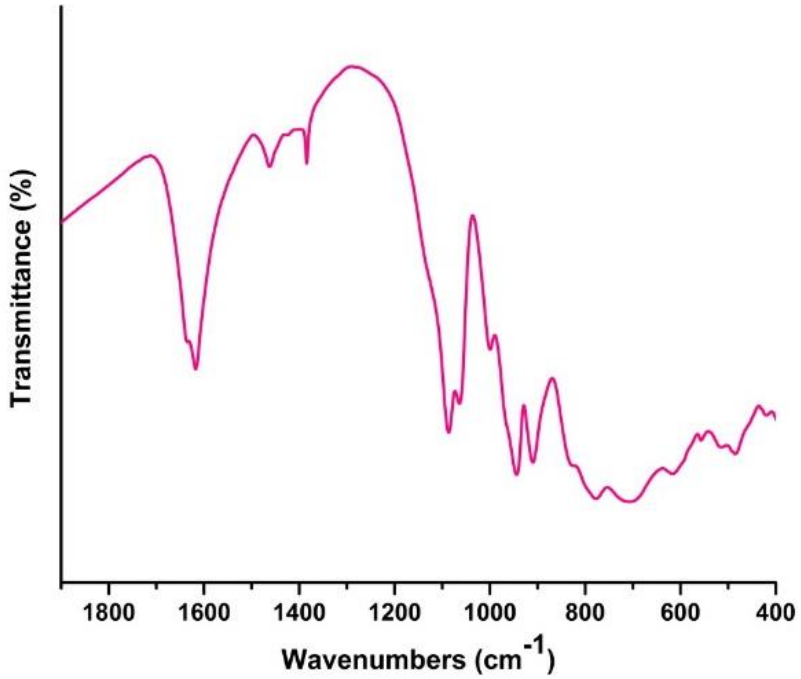

Figure S3. FT-IR spectrum of **K-Fe$_{48}$** (measured as a KBr pellet). The most important IR peaks are at ca 1200-1000 cm^{-1} (P–O bonds of the PO_4 hetero groups), ca 1000-800 cm^{-1} (terminal W-O bonds) and ca 800-600 cm^{-1} (bridging W-O-W bonds). The strong peak at 1617 cm^{-1} is attributed to lattice water molecules.

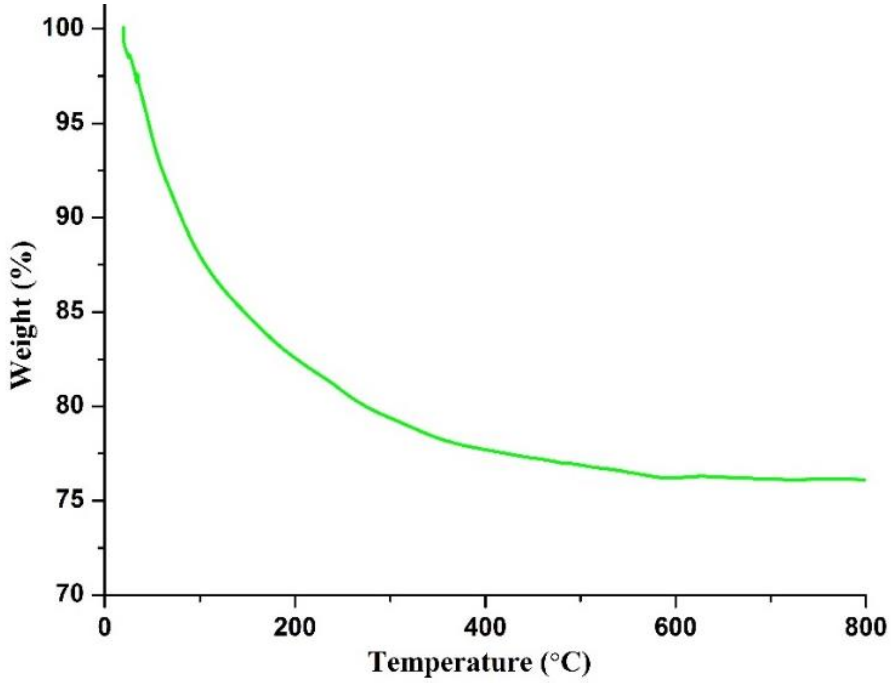

Figure S4. Thermogram of **K-Fe$_{48}$** from room temperature to 800 ºC under N_2.

Table S2. Bond valence sum (BVS) values for the iron atoms in **Fe$_{48}$**.[S7]

Atom	BVS	Ox. state		Atom	BVS	Ox. state
Fe1	3.04	+3		Fe25	2.83	+3
Fe2	3.03	+3		Fe26	3.16	+3
Fe3	3.02	+3		Fe27	3.04	+3
Fe4	3.06	+3		Fe28	3.11	+3
Fe5	2.99	+3		Fe29	3.05	+3
Fe6	2.89	+3		Fe30	3.00	+3
Fe7	3.07	+3		Fe31	3.15	+3
Fe8	3.27	+3		Fe32	3.26	+3
Fe9	2.97	+3		Fe33	3.21	+3
Fe10	3.22	+3		Fe34	3.22	+3
Fe11	3.06	+3		Fe35	2.96	+3
Fe12	2.83	+3		Fe36	2.96	+3
Fe13	3.08	+3		Fe37	3.00	+3
Fe14	3.10	+3		Fe38	3.21	+3
Fe15	3.36	+3		Fe39	3.12	+3
Fe16	3.04	+3		Fe40	3.14	+3
Fe17	2.94	+3		Fe41	3.05	+3
Fe18	3.28	+3		Fe42	3.10	+3
Fe19	3.16	+3		Fe43	3.00	+3
Fe20	3.11	+3		Fe44	3.08	+3
Fe21	2.91	+3		Fe45	3.13	+3
Fe22	2.95	+3		Fe46	3.04	+3
Fe23	2.84	+3		Fe47	3.07	+3
Fe24	3.19	+3		Fe48	3.15	+3

Table S3. BVS values for the monoprotonated oxygen atoms (Fe-OH-Fe bridges) in **Fe$_{48}$**.[S7]

Atom	BVS	Atom	BVS
O12R	1.34	O256	1.16
O13E	1.09	O58F	1.06
O14E	1.08	O56F	1.07
O25E	1.15	O57F	1.05
O23E	1.13	O69F	1.19
O45I	1.16	O65F	1.15
O42F	1.15	O67F	1.03
O46E	1.09	O74F	1.12
O50F	1.22	O89E	1.20
O56E	1.01	O280	1.16
O61F	1.08	O90F	1.00
O78E	1.23	O12I	1.18
O79E	1.08	O13F	1.13
O71F	1.09	O14F	1.12
O89R	1.15	O25F	1.21

O80F	1.12	O23F	1.23
O01F	1.03	O45F	1.12
O02R	0.95	O46R	1.12
O12E	1.13	O56R	0.95
O36F	1.13	O378	1.26
O34E	1.11	O79F	1.17
O35E	0.99	O70F	1.10
O32E	1.10	O81F	1.20
O47F	1.06	O89F	1.10
O44F	1.14	O02F	1.12
O45R	1.10	O01E	1.15
O53F	1.10	O48F	1.08
O67R	1.23	O417	1.07
O68E	1.10	O12F	0.95
O78I	1.22	O26F	1.06
O90E	1.22	O34R	1.16
O93F	1.11	O437	1.15
O91F	1.15	O35F	1.10
O02E	1.20	O45E	1.13
O01R	1.05	O46F	1.11
O23R	1.16	O67E	1.05
O24F	1.16	O68F	1.13
O34F	1.03	O78F	1.05

Table S4. BVS values for the diprotonated oxygen atoms (Fe-OH_2) in **Fe_{48}**.[S7]

Bond	**BVS**	**Bond**	**BVS**
Fe1- O1FE	0.36	Fe29- O29F	0.46
Fe2- O2FE	0.33	Fe20- O20F	0.43
Fe7- O7FE	0.53	Fe43- O43F	0.44
Fe8- O8FE	0.53	Fe37- O37E	0.46
Fe38- O38F	0.48	Fe28- O28F	0.47
Fe16- O16F	0.41	Fe19- O19F	0.45
Fe44- O44E	0.44	Fe31- O31F	0.52
Fe32- O32F	0.49	Fe17- O17F	0.42

Magnetism

The magnetic behavior of **Fe$_{48}$** could be described by a classical Heisenberg model with the following Hamiltonian:

$$\widehat{H} = \sum_{i,j=1}^{30} J_{ij}\widehat{\boldsymbol{S}}_{\boldsymbol{i}} \cdot \widehat{\boldsymbol{S}}_{\boldsymbol{j}}$$

in which J_{ij} is the exchange interaction constant between the i^{th} and j^{th} Fe^{3+} centers as shown in Figure S5 (lower). In order to ascertain the oxidation state and spin magnetic moment of the title polyanion, it was subjected to magnetization measurements on a polycrystalline sample of **K-Fe$_{48}$** using a SQUID magnetometer as discussed in our earlier reports.[S8]

Figure S5 (top) shows the field dependence of the magnetization at 1.8 K. The reduced magnetization ($M/N\mu_\beta$) increases with increasing field and does not saturate even at 7 T. Considering the observation of antiferromagnetic coupling the competing interactions do not allow for an assignment of the expected spin structure of the polyanion. The reduced magnetization ($M/N\mu_\beta$) increases almost linearly with the magnetic field above 3 T. In order to obtain a better understanding of the nonlinear part, the quasilinear part (shown in solid red line in Figure S5 (top) was subtracted from M. The resulting $M\text{-}M_{linear}$ is displayed in Figure S5 (bottom). The dotted line indicates the magnetization at H = 7 T. The saturation moment of M_s = 5.26 μ_β is close to 5 μ_β expected for a saturation of one Fe^{III} ion, indicating clearly that the iron ion is Fe^{III}. These results are consistent with the fact that the **K-Fe$_{48}$** does not exhibit any long-range ferro or antiferromagnetic ordering from 300 K down to 1.2 K.

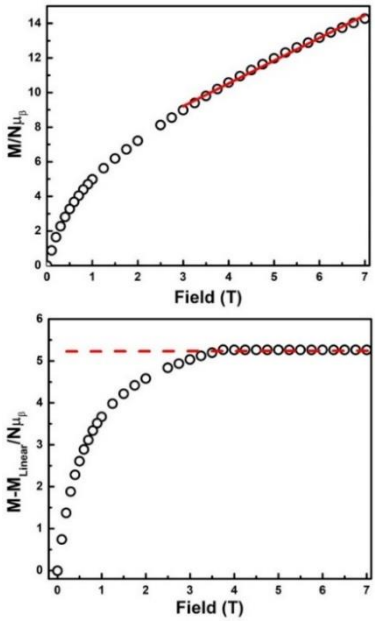

Figure S5. Field dependence of magnetization for **K-Fe$_{48}$** at 1.8 K (top); nonlinear part of M(H) (bottom).

Electrochemistry

Electrochemical measurements were performed using a CH Instruments Model 760D workstation (Austin, TX, USA) operating in three electrodes configuration. The glassy carbon working electrode was in a form of the disk of geometric area, 0.071 cm^2. The reference electrode was a saturated calomel electrode (SCE: Hg/Hg_2Cl_2, KCl), and a carbon rod was set as the counter electrode. All diagnostic electrochemical measurements were performed in 0.5 M KCl adjusted to pH = 2.

Deposits of $K_{28}[Fe_{48}(OH)_{76}(H_2O)_{16}(H_2P_2W_{12}O_{48})_8]\cdot 431H_2O\cdot 2KCl$ (**K-Fe$_{48}$**) and $K_{16}Li_4[Fe_{16}(OH)_{28}(H_2O)_4P_8W_{48}O_{184}]\cdot 66H_2O\cdot 2KCl$ (**KLi-Fe$_{16}$**, for comparison) were prepared by mixing 1 mg of these materials with 6 µl of water. Next, the obtained "paste" was rubbed onto the surface of a glassy carbon electrode or the microelectrode-based set-up (Figure S6). For the experiments in aqueous electrolyte, the deposit (on glassy carbon) was over-coated with an ultrathin film of Nafion polyelectrolyte (by introducing 1 µl of the Nafion solution (prepared by mixing 5% (mass) commercial Nafion solution with ethanol at a 1 to 10 volumetric ratio).

All solutions were prepared by using doubly-distilled and subsequently deionized (Millipore Milli-Q) water, which was deoxygenated by bubbling high-purity nitrogen for at least 30 min. During the microelectrode-based solid-state-type voltammetric measurements, the nitrogen gas (premium quality from Air Products) atmosphere was kept in the glass chamber surrounding the planar three-electrode configuration. The measurements were done at room temperature (22±2°C).

The title polyanion **Fe$_{48}$** contains two types of redox-active metals allowing for electron transfer, namely W^{VI}/W^{V} and Fe^{III}/Fe^{II}, which renders electrochemical experiments attractive. For Keggin- and Dawson-type heteropolytungstates the reduction of W^{VI} to W^{V} is expected to be fast and reversible.[S9-10] On the other hand, the supposedly outer-sphere redox transitions encompassing Fe^{III} sites in the gigantic polyanion **Fe$_{48}$** are likely more complex, reflecting their distinct chemical environments (*vide supra*). The electrochemical diagnostic experiments described here include both (i) conventional voltammetry of **K-Fe$_{48}$** dissolved in aqueous medium and (ii) microelectrode based solid-state-type methodology,[S11-13] to account for possible hydrolytic decomposition of the polyanion.

For our electrochemical experiments we used a glassy carbon electrode modified with deposited polyanion **Fe$_{48}$**, which was subjected to a voltammetric examination in 0.5 mol dm^{-3} KCl at pH 2 (Figure S7). Care was exercised to apply neither too negative nor too positive potentials, namely to avoid excessive hydrogen evolution or the system's physical degradation or dissolution. During the negative potential scans, at potentials lower than -0.2 V, reduction of

W^{VI} to W^{V} within the macrocyclic polytungstate ring occurs. The process is fast and reversible and, most likely, involves one-third of all tungsten sites (namely 32 W^{VI}). The actual reduction/oxidation voltammetric peaks appearing in the range from -0.3 to -0.7 V are almost symmetrical and have a surface-type character. The fact that they are not perfectly narrow (the width at half-height of both the cathodic and anodic peaks is around 150 mV, rather than the theoretically predicted 90.6/n mV, where n is the number of electrons involved),[S14] originates from the existence and overlap of numerous $W^{VI,V}$ redox transitions within the polytungstate ring. It is noteworthy that the electrochemical characteristics of the 16-Fe^{III}-containing $\{P_8W_{48}\}$ wheel $[Fe_{16}(OH)_{28}(H_2O)_4P_8W_{48}O_{184}]^{20-}$ (**Fe_{16}**),[S15] which we used as a reference, show a similar set of voltammetric peaks, when investigated as a deposit under identical experimental conditions (Figure S7, inset), but these bands are less symmetrical, which may imply some kinetic limitations. In the case of **Fe_{16}** the redox processes involving Fe^{III} (although not well defined) can be postulated, but there is no evidence for electroactivity of Fe^{III} in the title polyanion **Fe_{48}** when the deposit is in contact with aqueous electrolyte. Finally, in both cases, at potentials more negative than -0.8 V, hydrogen evolution becomes operative.

Due to a possible decomposition of **Fe_{48}** in aqueous medium we decided to also perform microelectrode-based solid-state electrochemistry on **K-Fe_{48}**. The diagnostic experiments were aimed at verifying the feasibility of fast and reversible electroreduction of W^{VI} to W^{V}, in addition to probing the redox transitions of the Fe^{III} ions in **Fe_{48}**.

The use of a microdisk electrode minimizes the so-called iR drops in cyclic voltammetry (CV) and permits reliable diagnostic measurements in the absence of external aqueous supporting electrolyte.[S16] When it comes to experiments with solid and semi-solid deposits, the overall charge propagation mechanism is based on electron hopping between mixed-valence ionic sites (*see main text*).[S17]

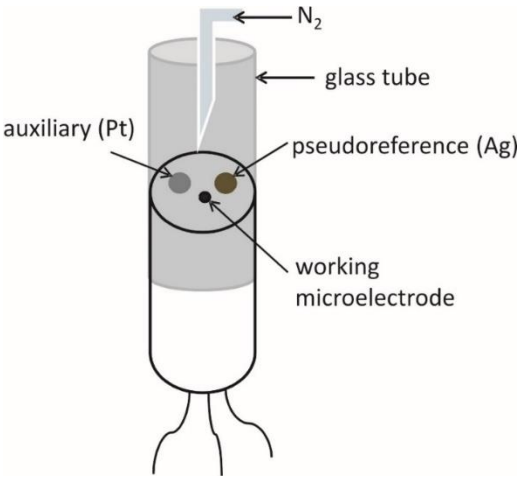

Figure S6. Schematic diagram of a microelectrode-based solid-state-type cell with a planar three-electrode configuration (measurement under nitrogen atmosphere).

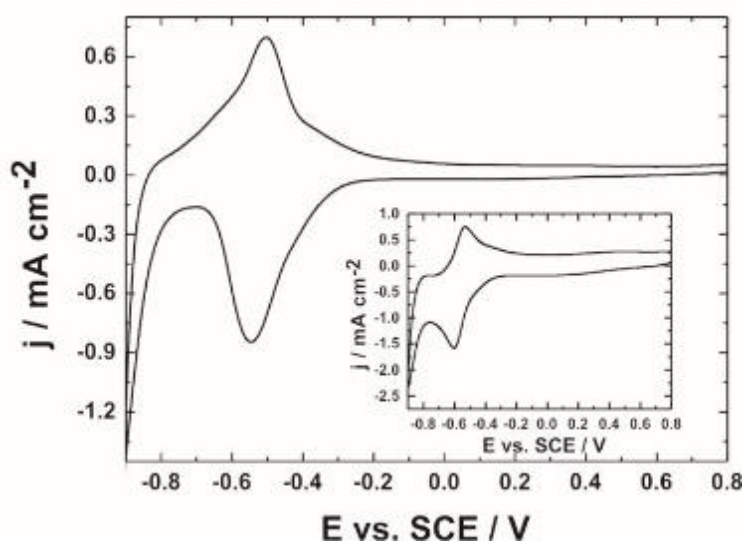

Figure S7. Cyclic voltammetric responses of **Fe$_{48}$** and, for comparison, **Fe$_{16}$** (inset).[S15] Electrode substrate: glassy carbon. Electrolyte: nitrogen-saturated 0.5 mol dm^{-3} KCl at pH = 2. Scan rate: 10 mV s^{-1}.

References

S1. R. Contant. *Inorg. Synth.* **1990**, *27*, 108.

S2. D. Foguet-Albiol, K. A. Abboud, G. Christou, *Chem. Commun*. **2005**, 4282-4284.

S3. *SAINT*; *Bruker AXS*, Inc.: Madison, WI, **2007**.

S4. a) G. M. Sheldrick, *Acta Crystallogr., Sect. A: Found. Crystallogr*. **2008**, *64*, 112−122; b) G. M. Sheldrick, *SADABS*; University of Göttingen: Göttingen, Germany, **1996**.

S5. a) G. M. Sheldrick, *SHELX-97/2013*: Program for Solution of Crystal Structures; University of Göttingen: Göttingen, Germany, **2013**; b) O. V. Dolomanov, L. J. Bourhis, R. J. Gildea, J. A. K. Howard, H. Puschmann, *J. Appl. Cryst.* **2009**, *42*, 339-341; c) G. M. Sheldrick, *Acta Cryst. A71*, **2015**, 3-8; d) G. M. Sheldrick, *Acta Cryst. C71*, **2015**, 3-8.

S6. D. Foguet-Albiol, K. A. Abboud, G. Christou, *Chem. Commun*. **2005**, 4282-4284.

S7. I. D. Brown, D. Altermatt, *Acta Cryst.* **1985**, *B41*, 244-247.

S8. K. Y. Wang, B. S. Bassil, X. Xing, B. Keita, J. K. Bindra, K. Diefenbach, N. S. Dalal, U. Kortz, *Eur. J. Inorg. Chem.* **2016**, 5519-5529.

S9. I. A. Rutkowska, P. J. Kulesza, *Encyclopedia of Interfacial Chemistry: Surface Science and Electrochemistry*, Elsevier, Amsterdam, 2018, pp. 651.

S10. P. J. Kulesza, L. R. Faulkner, *J. Am. Chem. Soc.* **1993**, *115*, 11878.

S11. P. J. Kulesza, M. A. Malik in Interfacial Electrochemistry: *Theory, Experiment and Applications, Solid-State Voltammetry* (Ed.: A. Wieckowski), Marcel Dekker, New York, 1999, pp. 673.

S12. P. J. Kulesza, J. A. Cox, *Electroanalysis* **1998**, *10*, 73.

S13. I. A. Rutkowska, M. Marszalek, J. Orlowska, W. Ozimek, S. M. Zakeeruddin, P.J. Kulesza, M. Grätzel, *ChemSusChem* **2015**, *8*, 2560.

S14. A. J. Bard, L.R Faulkner, *Electrochemical Methods*, VCH, New York, **1994**.

S15. a) R. Naseer, S. S. Mal, M. Ibrahim, U. Kortz, G. Armstrong, F. Laffir, C. Dickinson, M. Vagin, T. McCormac, *Electrochim. Acta* **2014**, *134*, 450; b) S. S. Mal, M. H. Dickman, U. Kortz, A. M. Todea, A. Merca, H. Bögge, T. Glaser, A. Müller, S. Nellutla, N. Kaur, J. van Tol, N. S. Dalal, B. Keita, L. Nadjo, *Chem. Eur. J.* **2008**, *14*, 1186-1195.

S16. a) P. J. Kulesza, J. A. Cox, *Electroanalysis* **1998**, *10*, 73; b) A. J. Bard, L. R. Faulkner, *Electrochemical Methods*, VCH, New York, 1994.

S17. N. A. Surridge, J. C. Jernigan, E. F. Dalton, R. P. Buck, M. Watanabe, H. Zhang, M. Pinkerton, T. T. Wooster, M. L. Longmire, J. S. Facci, R. W. Murray, *Faraday Discuss.* **1989**, *88*, 1.